Earth and Planetary Science Letters 401 (2014) 347–358

Contents lists available at ScienceDirect

Earth and Planetary Science Letters

www.elsevier.com/locate/epsl

A new model for the (geo)magnetic power spectrum, with application to planetary dynamo radii

Benoit Langlais [a,*], Hagay Amit [a], Hugo Larnier [a,b], Erwan Thébault [c], Antoine Mocquet [a]

[a] Laboratoire de Planétologie et Géodynamique, CNRS UMR 6112, Université de Nantes, 44322 Nantes cedex 3, France
[b] Institut de Physique du Globe de Strasbourg, UdS–CNRS UMR7516, EOST – Université de Strasbourg, 5 rue René Descartes, 67084 Strasbourg Cedex, France
[c] Équipe de Géomagnétisme, Institut de Physique du Globe de Paris, CNRS UMR 7154, 75252 Paris cedex 5, France

ARTICLE INFO

Article history:
Received 6 November 2013
Received in revised form 23 April 2014
Accepted 10 May 2014
Available online 9 July 2014
Editor: C. Sotin

Keywords:
magnetic power spectrum
dynamo radius
planetary structure

ABSTRACT

We propose two new analytical expressions to fit the Mauersberger–Lowes geomagnetic field spectrum at the core–mantle boundary. These can be used to estimate the radius of the outer liquid core where the geodynamo operates, or more generally the radius of the planetary dynamo regions. We show that two sub-families of the geomagnetic field are independent of spherical harmonics degree n at the core–mantle boundary and exhibit flat spectra. The first is the non-zonal field, i.e., for spherical harmonics order m different from zero. The second is the quadrupole family, i.e., $n+m$ even. The flatness of their spectra is motivated by the nearly axisymmetric time-average paleomagnetic field (for the non-zonal field) and the dominance of rotational effects in core dynamics (for the quadrupole family). We test our two expressions with two approaches using the reference case of the Earth. First we estimate at the seismic core radius the agreement between the actual spectrum and the theoretical one. Second we estimate the magnetic core radius, where the spectrum flattens. We show that both sub-families offer a better agreement with the actual spectrum compared with previously proposed analytical expressions, and predict a magnetic core radius within less than 10 km of the Earth's seismic core radius. These new expressions supersede previous ones to infer the core radius from geomagnetic field information because the low degree terms are not ignored. Our formalism is then applied to infer the radius of the dynamo regions on Jupiter, Saturn, Uranus and Neptune. The axisymmetric nature of the magnetic field of Saturn prevents the use of the non-zonal expression. For the three other planets both expressions converge and offer independent constraints on the internal structure of these planets. These non-zonal and quadrupole family expressions may be implemented to extrapolate the geomagnetic field spectrum beyond observable degrees, or to further regularize magnetic field models constructed from modern or historical observations.

1. Introduction

Inferring the internal structure of a planet is a major challenge in planetary exploration. This information is generally deduced from moment of inertia and seismic measurements (e.g., Mocquet et al., 2011), but seismic data are usually either not available or too sparse on planets other than the Earth. Moment of inertia alone does not allow to decipher density and thickness variations, and additional constraints or assumptions such as on the composition of the planetary bodies are necessary (e.g., Guillot, 2005). Inferred temperature and pressure radial distributions may be combined with experiments and equations of state to estimate the depth at which phase transitions occur (Fortney, 2007). Heat flow measurements, surface or atmosphere composition, and surface features also bring additional constraints (Hagermann, 2005; Zuber et al., 2010; Baraffe et al., 2014). The mass and radius of an exoplanet can eventually be combined to infer its water content or its class (Grasset et al., 2009).

Alternatively, planetary internal structure may be constrained by magnetic field measurements. Electromagnetic studies can indeed provide crucial information about the electrical conductivity of internal layers (Verhoeven et al., 2009; Civet and Tarits, 2013). Observed delay times of geomagnetic jerks may also constrain the electrical conductivity profile of the mantle (Pinheiro and Jackson, 2008). The size of the liquid core, or more generally of the electrically conductive and convecting layer where the magnetic field is generated, can also be inferred from measurements of the magnetic field and of its secular variation (Hide, 1978). This information is particularly useful when other constraints fail to unambiguously determine the internal structure of these bodies.

* Corresponding author.
E-mail address: benoit.langlais@univ-nantes.fr (B. Langlais).

http://dx.doi.org/10.1016/j.epsl.2014.05.013
0012-821X/

Lowes (1966) defined the so-called spatial power spectrum of the (geo)magnetic field. This quantity represents the energy of the magnetic field for a given spherical harmonics (SH) degree and is also known as the Lowes–Mauesberger spectrum (Lowes, 2007). In the case of the Earth, and assuming that the mantle is source-free, one can downward continue the magnetic field as predicted from SH models down to the core–mantle boundary (CMB). It has been observed that the magnetic power spectrum has two distinct parts (Lowes, 1974; Langel and Estes, 1982), separated by a knee around SH degree $n = 15$. For larger degrees the spectrum is almost flat at the Earth's surface. This has been interpreted as the spectrum being associated with the so-called 'white noise' hypothesis (Backus et al., 1996). For lower degrees, the spectrum becomes almost flat at the CMB. This well-known property provides an alternative way to estimate the size of the dynamo region, i.e., the depth at which the magnetic power spectrum becomes flat.

Based on paleomagnetic field analysis, Constable and Parker (1988) concluded that excluding the axial dipole and axial quadrupole, the remaining spectrum is flat at the CMB. This may be regarded as a statistical sample from a single giant Gaussian process (GGP). The GGP formalism was generalized by Hulot and Le Mouel (1994). Time-average paleomagnetic field and paleo secular variation modeling strategies rely on a GGP description (for a review see Hulot et al., 2010). In addition, it was shown that GGP describes well the field produced by numerical dynamo models (e.g., Bouligand et al., 2005). Following this rationale, it is therefore expected that some part of the spectrum will be flat immediately above the magnetic field sources (Backus et al., 1996).

Lowes (1974) used an empirical power law to describe the geomagnetic spatial power spectrum between $n = 3$ and 8 of the International Geomagnetic Reference Field (IGRF) 1965 (Zmuda, 1971), and found a core radius equal to 2995 km, to be compared to the commonly adopted seismic value of 3481.7 km (Dziewonski and Anderson, 1981; Kennett et al., 1995, hereafter denoted the seismic radius of the CMB). He attributed this low value to both the inaccuracy of the field model and to the severe model truncation. Using a field model based on MAGSAT measurements, Langel and Estes (1982) found a core radius of 3311 km for $n = 2$–12. A more elaborated SH model led to a depth of 80 km below the CMB, again omitting the $n = 1$ term (Cain et al., 1989).

A second expression is the so-called McLeod's rule, referring to the work of McLeod (1996). This approach is based on statistical considerations relating the spectrum of the magnetic field to that of the secular variation. Using this approach, Voorhies et al. (2002) estimated the radius of the outer core to be 30 or 70 km above the seismic one considering degree terms $n = 1$–12 or 1–13, respectively. Core radius estimates using McLeod's rule are even closer to the seismic radius when omitting degrees 1 and 2 (Voorhies, 2004).

These two different expressions offer two slightly different estimates of the Earth's liquid core radius. However none of these expressions can satisfactorily predict it. More importantly the question remains which degrees deviate from the flat spectrum hypothesis, or from the chosen analytical expression. In this study we suggest that the flat spectrum hypothesis applies for specific sub-families of the (geo)magnetic power spectrum, and propose two new analytical expressions of the (geo)magnetic spatial power spectrum. These two sub-families are the non-zonal and the quadrupole family.

In the following we present in Section 2 the existing and new analytical expressions of the (geo)magnetic spatial power spectrum. In Section 3 we describe the statistical tools used to test and compare the analytical expressions. Results of those tests on geomagnetic field models are given in Section 4, including dependencies on the truncation degree, the geomagnetic field model epoch and geomagnetic field model level of parametrization. We apply our new analytical expressions to the gas giant planets in Section 5 and conclude in Section 6.

2. Analytical expressions of the geomagnetic spatial power spectrum and core radius estimate

Outside a magnetic source region, the magnetic field vector $\vec{B}$ can be written as the gradient of a scalar potential V which satisfies Laplace's equation:

$$\nabla^2 V = 0 \tag{1}$$

Gauss (1839) showed that the potential associated with internal sources can be written as a SH expansion:

$$V_{int}(r,\theta,\phi) = a\sum_{n=1}^{\infty}\sum_{m=0}^{n}\left(\frac{a}{r}\right)^{n+1} \times \left(g_n^m \cos m\phi + h_n^m \sin m\phi\right) P_n^m(\cos\theta) \tag{2}$$

where (r,θ,ϕ) are the spherical coordinates radius, colatitude and longitude, g_n^m and h_n^m are the time-dependent internal field Gauss coefficients (in nanoTesla, nT) of degree n and order m, a is Earth's mean spherical radius and P_n^m are the Schmidt semi-normalized associated Legendre functions. We note that these expressions are valid for other planets, by simply substituting the appropriate planetary radius for a.

The potential V_{int} accounts for the magnetic sources located below the measurement altitude. In the case of magnetic measurements acquired at or above the surface of the Earth, this potential encompasses the internally generated geodynamo field, remanent field, induction effects in the lithosphere and in the mantle. This expansion is infinite, but it is usually truncated to some finite degree N_{int} (Langel, 1987).

At the Earth's surface, the mean square magnetic field of degree n, denoted here $R_n(a)$, is expressed as (Lowes, 1966):

$$R_n(a) = (n+1)\sum_{m=0}^{n}\left(\left(g_n^m\right)^2 + \left(h_n^m\right)^2\right) \tag{3}$$

The quantity R_n is the geomagnetic spatial power spectrum. It can be upward or downward continued, as long as Eq. (1) is respected. One can write $R_n(r)$:

$$R_n\left(r, r \geq r_c^s\right) = R_n(a)\left(\frac{a}{r}\right)^{2n+4} \tag{4}$$

where r_c^s is the seismic radius of the outer core (presumably that of the dynamo region). The behavior of the geomagnetic power spectrum at the Earth's CMB is shown in Fig. 1(a). At the CMB, the spectrum of the core field remains more or less flat. In this study we are interested by the core portion of the geomagnetic spatial power spectrum only.

The average squared magnetic field over a spherical surface of radius r is equal to the sum (over n) of the individual terms of Eq. (4):

$$\left\langle\left|\vec{B}(r)\right|^2\right\rangle = \sum_{n=1}^{N_{max}} R_n(a)\left(\frac{a}{r}\right)^{2n+4} \tag{5}$$

where N_{max} is the maximum SH degree considered. Because the magnetic field is a finite quantity, as long as the magnetic sources lie below this spherical surface, and assuming that the trend of the spectrum is unchanged beyond N_{max}, all individual terms $R_n(a)$ are bounded (e.g., Backus et al., 1996), such as

$$R_n(r) \leq C\left(\frac{r}{a}\right)^{2n+4} \tag{6}$$

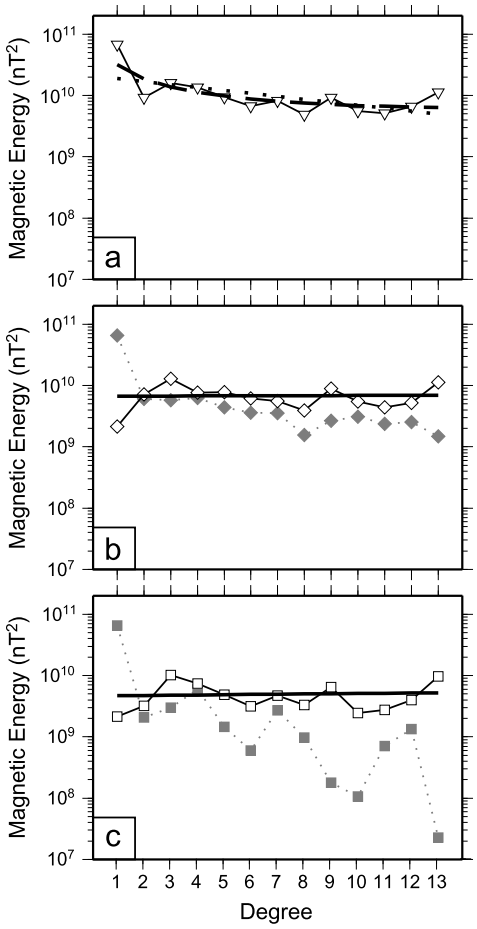

Fig. 1. Geomagnetic spatial power spectra of the CHAOS4α field model at epoch 2005 at the CMB. (a) Full spectrum (symbols) with power law (thick dotted line) and McLeod's rule fits (thick dashed line); (b) non-zonal (open symbols) and zonal (gray closed symbols) spectra with non-zonal expression fit (thick line); (c) quadrupole (open symbols) and dipole (gray closed symbols) family spectra with quadrupole family expression fit (thick line). All graphs are plotted with the same scale.

where C is a given constant. Their sum (Eq. (5)) is bounded too. Given a theoretical model for $R_n(r)$ and a geomagnetic core field model with sufficient accuracy for $R_n(a)$, it is thus possible to estimate the maximum distance to the magnetic sources by looking for the smallest value of r at which the series $R_n(r)$ remains a decreasing function, or even becomes flat and independent of n. There is of course some n at which a flat spectrum will not be valid anymore, as there is some finite magnetic energy. Any extrapolation to high degree is limited by the magnetic dissipation scale, from which the spectrum is expected to rapidly decay. The spherical harmonic degree corresponding to the magnetic dissipation scale is estimated to be about 150 (Christensen and Tilgner, 2004; Buffett and Christensen, 2007; Finlay and Amit, 2011). This is much larger than the typical truncation degree of core field models and will be ignored in the following.

2.1. Previously proposed expressions: power law and McLeod's rule

The shape of the spectrum associated with the core field is empirically approximated by a power law. This was first introduced by Lowes (1974), such as

$$R_n^{pl}(r) = A_1 \cdot B_1^n \tag{7}$$

The superscript pl stands for the power law expression, and A_1 and B_1 denote empirically determined constants (in the following, A_i, B_i and C_i denote constants and their ln). This expression was used in different forms by several authors (e.g., Langel and Estes, 1982; Cain et al., 1989; Roberts et al., 2003; Buffett and Christensen, 2007). Taking the logarithm of Eq. (7),

$$\ln R_n^{pl}(r) = A_1 + n \cdot B_1 \tag{8}$$

the 'magnetic' radius r_c^m is found by equating $\ln R_n^{pl}(r_c^m)$ to a constant. We note that this quantity may be different from the seismic value of the core radius r_c^s.

McLeod (1996) introduced a different expression to explain the geomagnetic spectrum. He proposed that the magnetic field sources can be statistically represented by horizontal magnetic dipoles (or magnetic monopoles) located at the base of each field line; he further suggested that the secular variation may be explained by horizontal magnetic dipoles, whose directions depend on the fluid flow. He finally related the spatial power spectrum of this secular variation to that of the main magnetic field (see Eqs. (12) to (20) of McLeod, 1996). Voorhies et al. (2002) generalized the so-called McLeod's rule to become

$$R_n^{mc}(r) = K \frac{n+1/2}{n(n+1)} \left(\frac{r}{a}\right)^{2n+4} \tag{9}$$

where K is empirically determined. At the CMB, using some simple algebra and applying ln on both sides, this can be rewritten as:

$$\ln\left(\frac{n(n+1)R_n^{mc}(r_c^s)}{n+1/2}\right) = A_2 + n \cdot B_2 \tag{10}$$

The linear regression of this equation leads to the estimate of r_c^m by looking for $B_2 = 0$, i.e., when $\ln(n(n+1)R_n^{mc}(r_c^m)/(n+1/2))$ is constant and independent of n. Note that the expression $R_n^{mc}(r_c^m)$ is not constant.

2.2. New analytical expressions: non-zonal and quadrupole family

We propose two alternative expressions motivated by the behavior of geomagnetic field models and supported by physical arguments. The first one is motivated by time-averaged paleomagnetic field models indicate that the magnetic field is mostly axisymmetric (Kono et al., 2000), and that non-zonal terms are weak and tend to average out. The non-zonal field can thus be seen as random at a given time, and when converted into SH, its spectrum has a null slope. We therefore propose that the non-zonal magnetic field spectrum R_n^{nz} (i.e., terms with $m \neq 0$):

$$R_n^{nz}(r) = \left(\frac{a}{r}\right)^{2n+4} (n+1) \sum_{m=1}^{n} \left(\left(g_n^m\right)^2 + \left(h_n^m\right)^2\right) \tag{11}$$

can be assumed to be independent of n, with:

$$R_n^{nz}\left(r_c^m\right) = C_3 \tag{12}$$

At the seismic core radius a more generic linear relation is written:

$$R_n^{nz}\left(r_c^s\right) = A_3 + n \cdot B_3 \tag{13}$$

The second expression is based on estimates of the magnitude of the Coriolis force with respect to the viscous and inertial forces, which suggest that the dynamics within Earth's outer core is strongly dominated by rotational effects (e.g., Olson, 2007). In the limit of rapidly rotating fluids the flow is expected to be organized in axial columns symmetric about the equator (Busse, 1970; Taylor, 1971; Jault, 2008). A columnar cyclone associated with CMB downwellings is expected to concentrate a pair of field structures of opposite polarities at the same longitude in opposite latitudes, thus

contributing to an anti-symmetric field (for schematic illustrations see Olson et al., 1999; Aubert et al., 2008). It is therefore likely that a symmetric core flow will induce an anti-symmetric magnetic field on the CMB. Such field is also known as the dipole family one. Decomposition to dipole and quadrupole families (Roberts, 1971; Gubbins and Zhang, 1993) was previously invoked to explain various dynamo processes, e.g., geomagnetic dipole decrease (Amit and Olson, 2010), geomagnetic reversals (Coe and Glatzmaier, 2006) and solar magnetic reversals (DeRosa et al., 2012).

In the following we propose that the action of the Coriolis force on core dynamics is responsible for the dominantly anti-symmetric field, and that the remaining symmetric field constitutes a deviation and can be seen as random. This motivates examining the quadrupole family spectrum R_n^{qf} (i.e., $n+m$ even) following:

$$R_n^{qf}(r) = \left(\frac{a}{r}\right)^{2n+4} (n+1) \sum_{m=0,\ n+m\ even}^{n} \left(\left(g_n^m\right)^2 + \left(h_n^m\right)^2\right) \tag{14}$$

We further suggest that this spectrum has a null slope immediately above the dynamo, leading to:

$$R_n^{qf}\left(r_c^m\right) = C_4 \tag{15}$$

At the seismic core radius a form similar to Eq. (13) leads to:

$$R_n^{qf}\left(r_c^s\right) = A_4 + n \cdot B_4 \tag{16}$$

The spectra associated with these two new sub-families are shown in Fig. 1(b) and (c), together with their zonal and dipole family counterparts, respectively. As expected the non-zonal and the quadrupole family spectra indeed appear to be more or less constant with an almost null slope. Both the zonal and dipole family spectra decrease relatively fast with increasing n, respecting Eq. (6).

3. Statistical tests of the expressions

The two new expressions are tested and compared to the two previously proposed ones. It is necessary to define some statistical criteria to evaluate their pertinence. Two kinds of tests are performed. First we estimate the misfit at the seismic CMB between the actual values of the geomagnetic spatial power spectrum and the predicted ones. Second we estimate how accurately the analytical expressions predict the magnetic core radius. These two statistical measures are finally combined into a quality factor.

The agreement between each analytical expression for the geomagnetic spatial power spectrum and the downward continued one at the CMB is evaluated by their normalized root mean square difference:

$$\sigma_s = \sqrt{\left(\frac{1}{N_{max} - N_{min}} \frac{\sum_{n=N_{min}}^{N_{max}} [R_n^{obs}(r_c^s) - R_n^{mod}(r_c^s)]^2}{\sum_{n=N_{min}}^{N_{max}} [R_n^{obs}(r_c^s)]^2}\right)} \tag{17}$$

where R_n^{mod} refers to one of the four expressions (Eqs. (8), (10), (12) and (15)) and R_n^{obs} refers to the observed full, non-zonal, or quadrupole family spectra. The dependence on the minimum and maximum SH degrees N_{min} and N_{max} is also considered. The misfit is normalized by $\sum_{n=N_{min}}^{N_{max}} [R_n^{obs}(r_c^s)]^2$ to allow proper comparison among the four expressions.

The second test considers the magnetic estimate of the depth to the magnetic sources, using Eqs. (7), (9), (13) and (16). The error is expressed in a relative way:

$$\sigma_m = \frac{r_c^s - r_c^m}{r_c^s} \tag{18}$$

This quantity may thus be negative or positive, although we note that overestimating the core radius may be seen as less erroneous than underestimating it from a physical point of view (it is indeed possible to downward continue the geomagnetic field power spectrum down to the CMB, but not below it).

Both the misfit at the CMB and the magnetic estimate of the core radius are important in order to assess the adequacy of the existing and proposed expressions. We therefore define an empirical combined quality factor,

$$\sigma_Q = \frac{1}{2}\sigma_s^* + \frac{1}{2}|\sigma_m^*| \tag{19}$$

We choose to normalize σ_s and σ_m because they can differ by several orders of magnitude. Normalization values are set so that they are equal to 1 for model CHAOS4α at epoch 2005 (see below) with $N_{max} = 8$ (normalization factors are 0.19793 and 12.25614, respectively). In addition the absolute value for σ_m^* is considered because a large negative σ_m^* could artificially balance a large σ_s^* value, resulting in an erroneously low σ_Q.

4. Application to the Earth's magnetic field

The tests are applied to four geomagnetic field models. Their main characteristics are given in Appendix A. These models represent different modeling strategies, datasets and validity epochs. We test the two new expressions and compare them to the existing ones. We focus on the sensitivity to truncation degree, model choice and model epoch.

4.1. Dependence on the maximum truncation degree

We start by applying the four expressions to model CHAOS4α at epoch 2005. We show in Fig. 2(a)–(c) the evolution of σ_m, σ_s and σ_Q for N_{max} varying between 6 and 14 ($N_{min} = 1$). The two new expressions offer better results for both the core radius and the misfit at the CMB. The non-zonal and quadrupole family expressions are associated with a minimum σ_Q for $N_{max} = 13$ or 14. Specifically, the results for $N_{max} = 13$ are given in Table 1. We also determine the accuracy of the estimated dynamo radius (Appendix B). The magnetic estimate of the core radius using the non-zonal and quadrupole family expressions is 3486.6 and 3496.6 km, respectively. This decreases the error on the core radius by one order of magnitude. The misfit at the seismic CMB is also slightly better. Dependence on N_{min} is also considered in Appendix C. In the following we set N_{min} and N_{max} to 1 and 13, respectively, unless specified.

4.2. Dependence on the field model

Next we apply the four expressions to the four different field models. These models do not cover the same time periods so we examine different epochs: 2005 for CHAOS4α, 2000 for CM4 and IGRF, and 1980 for gufm1. We present the results in Fig. 3.

As for the truncation degree test, the two new expressions offer significantly better results than the power law and McLeod's rule for all models except for gufm1 (see below). The three more recent models present similar results, with the two non-zonal and quadrupole family expressions offering both a better estimate of the core radius and a better fit to the spectrum. Core radius estimates associated with CHAOS4α model can also be found in Table 1. The CM4 and IGRF field models lead to core radius estimate errors ranging between −4.6 and 17.1 km using the newly proposed expressions. For gufm1 the best results are obtained by McLeod's rule. We further investigate this field model, and in particular the time-dependence issue, in the following subsection.

Table 1
Relative error on core radius estimate σ_m, misfit at the CMB σ_s, and combined quality factor σ_Q associated with the four expressions from field model CHAOS4α at epoch 2005 and for $N_{max} = 13$. Last three columns show the magnetic core radius estimate r_c^m, its standard deviation and minimum/maximum (all in km).

Expression	σ_m	σ_s	σ_Q	r_c^m	std	*min/max*
Power law	−5.376	0.186	0.689	3294.5	3.1	94.8/116.1
McLeod's rule	3.009	0.140	0.477	3586.5	3.2	−196.3/−176.7
Non-zonal	0.141	0.107	0.276	3486.6	4.7	−8.0/20.7
Quadrupole family	0.430	0.129	0.342	3496.7	5.9	−4.5/34.9

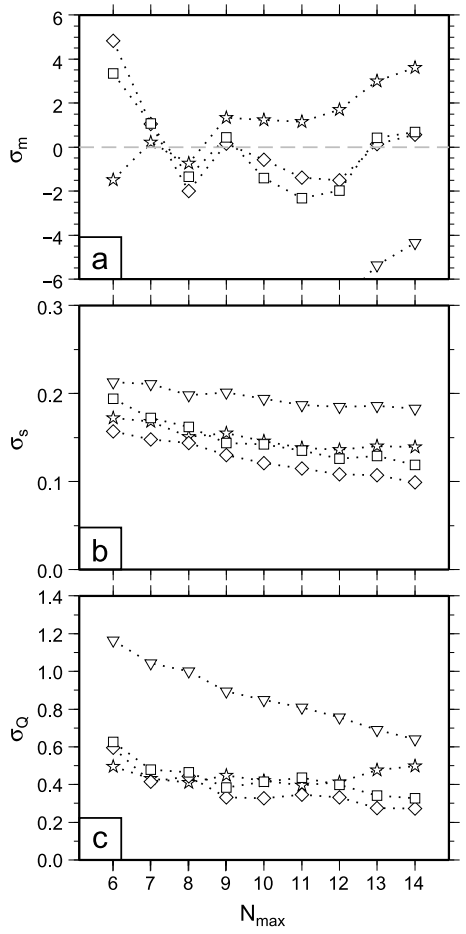

Fig. 2. Evolution of σ_s ((a), Eq. (17)), σ_m ((b), Eq. (18)) and σ_Q ((c), Eq. (19)) for a varying N_{max} for field model CHAOS4α at epoch 2005, and for the power law (inverted triangles), McLeod's rule (stars), non-zonal (diamonds) and quadrupole family (squares) expressions fits.

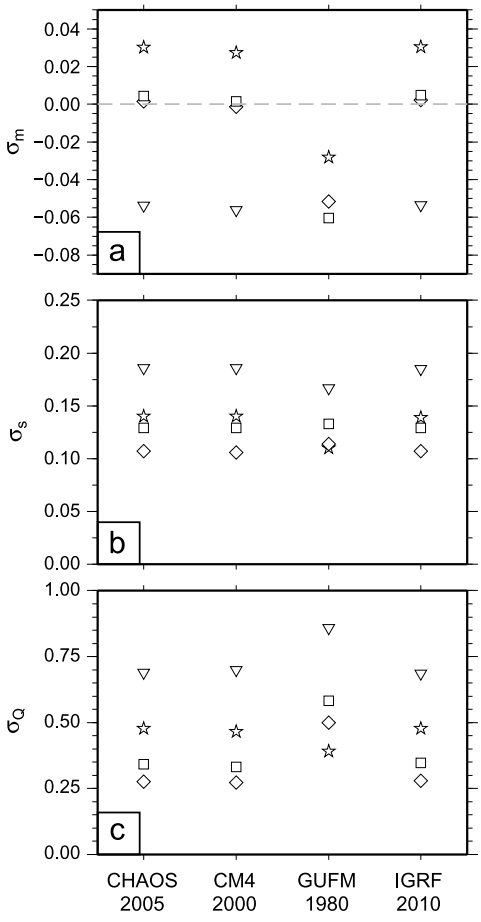

Fig. 3. Same as Fig. 2 for the four described magnetic field models.

4.3. Time-dependence

With the exception of model gufm1 at epoch 1980, our tests show that the two new proposed expressions offer better approximations to the geomagnetic spatial power spectrum at a given time. In the following we test the time-dependence of these statistics.

We show in Fig. 4 the behavior of σ_Q for the four tested field models as a function of the model epoch. Results associated with the CHAOS4α model series exhibit very little change, lower than 0.01 for the 13-yr long interval (Fig. 4(a)). A similar behavior can be observed for the CM4 field model (Fig. 4(b)). There is no particular trend over the considered 40-yr long interval, with for instance a minimum value observed in 1995 (0.337) and a maximum in 1975 (0.368) for the quadrupole family expression. For these two field models the non-zonal expression gives a slightly lower σ_Q than the quadrupole family expression. McLeod's rule and the power law are associated with larger misfits.

The longer series of IGRF and gufm1 show different results. IGRF models are available up to $N_{max} = 10$ until 1995 and $N_{max} = 13$ thereafter (Figs. 4(c1) and (c2) for a zoom over this last period). There is more variability in the results. Prior to 1940 there is a smooth variation of σ_Q. In 1945 and 1950, there is a clear jump; this can be associated with the peculiar behavior of IGRF models at these epochs as reported by Xu (2000). After 1955 the evolution of σ_Q is less monotonic than before 1940. As for CHAOS4α and CM4, the non-zonal and quadrupole family expressions provide better approximations to the geomagnetic spatial power spectrum and better estimates of the core radius. We also compare the results for $N_{max} = 10$ and 13 after 2000. Taking into account these three additional terms leads to better results, except for McLeod's rule. However it is worth noting that σ_Q is poorer for IGRF than for CM4 or CHAOS4α at similar epochs.

Finally we consider the gufm1 field model series. Prior to 1840, there were no magnetic observatories at the surface of the Earth (Barraclough, 1974; Bloxham and Jackson, 1992), so we chose to focus only on the 1840–1990 period. Two different N_{max} values are tested, namely 8 and 13. Before 1940, field models up to $N_{max} = 8$

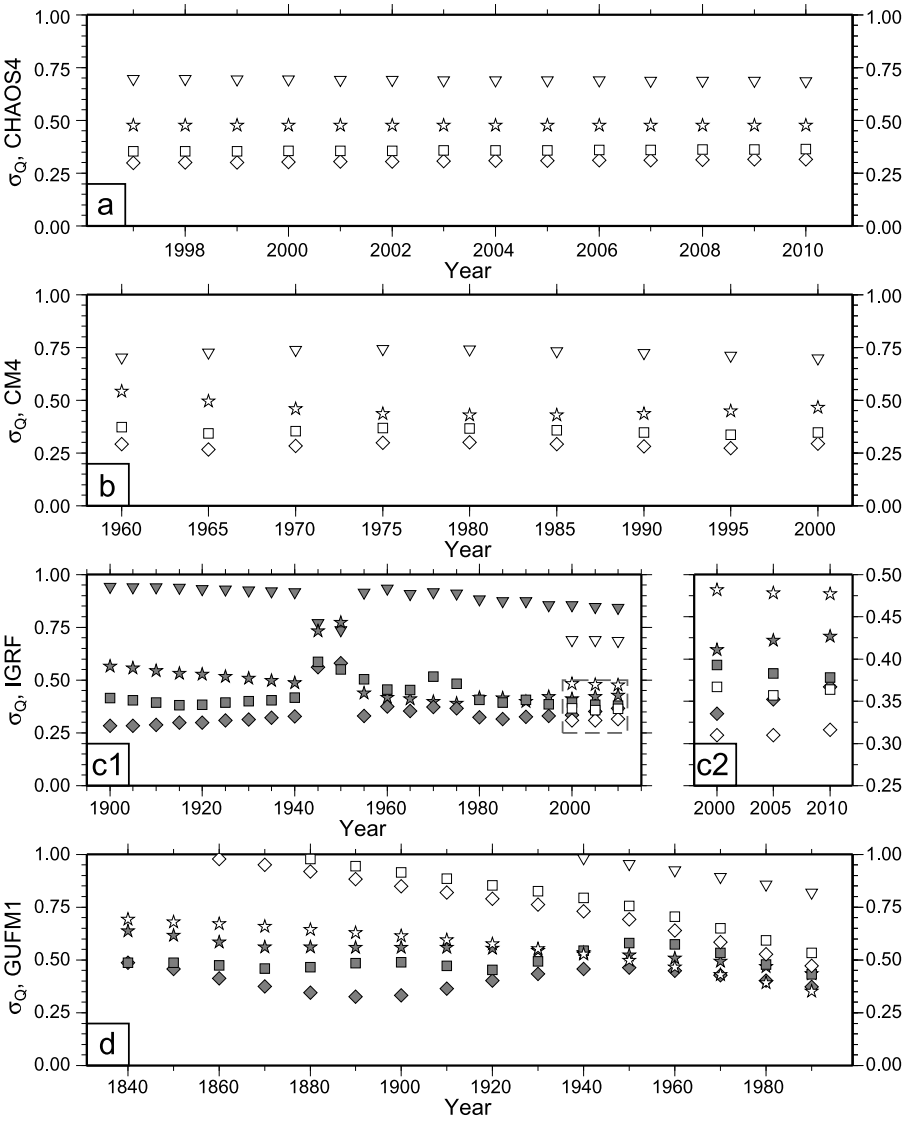

Fig. 4. Quality factor σ_Q as a function of time for four different field models: power law (inverted triangles), McLeod's rule (stars), non-zonal expression (diamonds) and quadrupole family expression (squares). (a) CHAOS4α from 1997 to 2010: 1-yr time interval, $N_{max} = 13$; (b) CM4 from 1960 to 2000: 5-yr time interval, $N_{max} = 13$; (c1) IGRF from 1900 to 2000: 5-yr time interval, $N_{max} = 10$ (closed symbols) or 13 (opened symbols); (c2) zoom of (c1) from 2000 to 2010; (d) gufm1 from 1840 to 1990: 10-yr time interval, $N_{max} = 8$ (closed symbols) or 13 (opened symbols).

are better fitted (lower σ_Q) than those up to $N_{max} = 13$. After 1960 the lowest misfit is obtained for McLeod's rule when $N_{max} = 13$ and by the non-zonal expression when $N_{max} = 8$. In 1980 the lowest σ_Q remains $\simeq$30% larger than for CM4 model at the same epoch.

There is a clear difference between CM4, CHAOS4α, IGRF and gufm1 series at similar epochs. The first two series have very steady results. Between 2000 and 2010 the evolution of the results should be identical between IGRF and CHAOS4α models if it was due to the evolution of the geomagnetic field rather than to the quality of the model: we find identical σ_Q in 2005 and 2010, but different, worse misfits in 2000 for IGRF. This is similarly observed before 1980 in IGRF series. It is likely that the temporal variability seen in that model series and in the entire gufm1 series is due to variations in the quality of the field models rather than to the genuine temporal evolution of the geomagnetic field.

5. Planetary applications

In the previous sections we proposed, tested and validated two new expressions to both predict the shape of the magnetic field power spectrum (or at least of two sub-families of it) and to estimate the distance to the magnetic sources (or the core radius for the Earth) using magnetic information only. This is an especially valuable information on other planets, where only remote measurements are available.

The only other terrestrial planet with a global and active magnetic field of internal origin is Mercury (Anderson et al., 2011). However we cannot currently apply our method to this planet, because there is no spherical harmonics model of the Hermean magnetic field. This is mainly due to the particular orbit of the MESSENGER spacecraft around Mercury: it has a nearly polar but very eccentric orbit, and no measurements are acquired close enough to the planet above the southern hemisphere, making it very challenging to compute global models (Johnson et al., 2012).

The magnetic fields of Jupiter, Saturn, Uranus and Neptune have been partly surveyed by different missions. Based on these measurements, global field models were derived. In the following we briefly summarize available magnetic field measurements and models as well as existing interior models, before attempting to estimate their planetary dynamo region radii.

5.1. Jupiter

The interior of Jupiter is commonly described by a three-layer structure, with a deep-seated core, a surrounding envelope of metallic hydrogen and an outermost layer of molecular hydrogen (e.g., Guillot, 2005). The internal structure is mainly constrained by geodesy and high pressure experiments. The inner core is solid, and smaller than 0.15 Rj (Jupiter radius, 1 Rj = 69 911 km) with a mass ranging between 7 and 18 Earth masses. The metallic hydrogen layer is the most likely source of the Jovian dynamo. Under the large pressure inside the deep interior of Jupiter, it is indeed expected that hydrogen is present in the form of a metallic liquid. The transition between the molecular and metallic hydrogen layers is not sharp. Different studies place the depth at which this transition occurs between 0.73 and 0.90 Rj (Gudkova and Zharkov, 1999; Guillot, 1999; Saumon and Guillot, 2004), with a transition layer of up to 0.1 Rj. This transition layer is however not thought to contribute to the dynamo which generates the magnetic field of Jupiter.

The Jovian system has been flown by several missions between 1973 and 2003. Measurements were acquired either during flybys (Pioneer 10, Pioneer 11, Voyager 1, Voyager 2, Ulysses) or by an orbiting spacecraft (Galileo, from 1995 to 2003). Several studies used these measurements to model the jovimagnetic field. Most models used only partial datasets: for instance Smith et al. (1975) used Pioneer 11 data only, whereas Connerney (1992) combined Pioneer 11 and Voyager 1 data. The position of the Io Flux-Tube (IFT) footprint as observed from the Earth or from Hubble Space Telescope was also used as an additional constraint (Connerney et al., 1998). Two models were computed using these data. VIP4 used in situ Voyager 1 and Pioneer 11 measurements, completed by 100 observations of the IFT. VIT4 used more than 500 IFT locations, completed by the north-south magnetic field component of the Voyager 1 measurements, as they are the least influenced by external field.

Given the 30-yr period over which magnetic field measurements were acquired (although not continuously), some attempts have been made to investigate the temporal variation of the jovimagnetic field. Using early datasets, some authors concluded that there were no evidence of a jovimagnetic secular variation (Connerney and Acuña, 1982; Dougherty et al., 1996). After the end of the Galileo mission Yu et al. (2010) compared the magnetic field as it had been modeled up to $N_{max} = 2$ from Galileo measurements to models derived from older measurements. They concluded that no secular variation could be unambiguously detected between Galileo's and older epochs.

In a more recent work (Ridley and Holme, 2012; Ridley, 2012), all existing measurements within 12 Rj of the planet were combined and integrated into two distinct models. Available measurements were mainly collected at equatorial latitudes. As a consequence the SH models of the Jovimagnetic field are limited in terms of their maximum degree. The first model is a time averaged model, denoted JTA and contains only main field Gauss coefficients. The second model is time dependent, denoted JSV and contains both main field and secular variation Gauss coefficients. Ridley (2012) conducted a thorough comparison of the different models for varying parameters and maximum SH degree. They concluded that the JSV model is statistically superior to the JTA model. The main field and secular variation of their JSV model is considered to be reliable up to degree 5 and 2, respectively. The magnetic power spectrum of this JSV model is shown at Jupiter's surface in Fig. 5(a).

Using the power law expression, Ridley (2012) visually estimated the depth at which the spectrum becomes flat, and returned a dynamo radius at 0.75 Rj for $N_{max} = 2$, and between 0.80 and 0.85 Rj for $N_{min} = 2$ and $N_{max} = 5$. We present in Table 2 the estimates of the dynamo radius using the four expressions for N_{max} ranging between 3 and 6. The power law and McLeod's rule offer systematically lower radius estimates than the two new expressions. The results of the new expressions are not plausible for $N_{max} = 3$ and 4 (i.e., with dynamo radius exceeding 1 Rj), but they become similar and converge for higher degree truncation. For $N_{max} = 5$ (the maximum reliable degree considered by Ridley, 2012) the dynamo region would be confined in a layer with a radius of 0.88 Rj. Other Jovian magnetic field models with $N_{max} = 4$ are also considered. Using the VIP4 model we obtain unplausible dynamo radii larger than 1 Rj. The non-zonal and the quadrupole family expressions converge to a dynamo radius equal to 0.84 Rj for the VIT4 model.

We compare in Fig. 5(b) and (c) the predicted power spectra for the non-zonal and quadrupole family expressions to the observed ones for the JSV model of Ridley (2012). This independent estimate at 0.88 Rj for the dynamo radius is very close to the upper value of the molecular to metallic transition radius, and may thus be used to further discriminate between different interior models of Jupiter.

5.2. Saturn

The interior of Saturn is thought to be very similar to that of Jupiter. There is a central core whose size is uncertain (Guillot, 2005; Nettelmann et al., 2013b). The core is surrounded by an inner metallic hydrogen layer and an outer molecular hydrogen layer. The transition between these two layers is, as for Jupiter, not sharp (Guillot, 2005). The radius at which the molecular-to-metallic transition of hydrogen takes place is generally located close to 0.6 Rs (Saturn radius, 1 Rs = 60 268 km) (Gudkova and Zharkov, 1999; Fortney, 2007). The dynamo has its origin in the metallic hydrogen shell, but it is uncertain whether the entire metallic hydrogen layer convects, as there could exist a transition layer (mixed molecular/metallic hydrogen) or stable stratified layer at the top of the convective region (Stevenson, 1980, 1983; Guillot, 2005; Christensen and Wicht, 2008; Stanley and Mohammadi, 2008) which would confine the dynamo to the deeper layer.

The magnetic field model of Saturn is mostly constrained by Cassini measurements, although some flyby measurements by other spacecrafts are available (Smith et al., 1980; Ness et al., 1981, 1982). Saturn's magnetic field is very axisymmetric, and no non-zonal field can be detected (Cao et al., 2011). The most recent model uses the previous model as a priori and further assumes a purely axisymmetric field up to degree 5, i.e., only zonal Gauss coefficients are solved for (Cao et al., 2012). The magnetic power spectrum of this field model is shown at Saturn's surface in Fig. 5(d). Cao et al. (2012) estimated the dynamo radius at 0.4 Rs when omitting the dipole term (i.e., using the power law for $N_{min} = 2$ and $N_{max} = 5$).

Here the non-zonal expression cannot be used, and only two Gauss coefficients can be used for the quadrupole family expression, i.e., g_2^0 and g_4^0. Using these two terms only, the estimated dynamo radius is found at 0.23 Rs (Table 3 and Fig. 5(e)). Cao et al. (2012) indicated that the error on their estimated g_4^0 coefficient is of the same magnitude as the coefficient ($g_4^0 = 65 \pm 70$ nT). Taking into account this error in our approach leads to a dynamo region radius ranging between 0.06 and 0.33 Rs. It is difficult to further assess the accuracy of this estimate. For comparison, a similar approach on the Earth, using an axisymmetric geomagnetic field model up to $N_{max} = 5$ would lead to a core radius of 0.62 Re (using the power law expression) or 0.71 Re (using only g_2^0 and g_4^0 in the quadrupole family expression as in the case of Saturn). The error on the Earth would thus be of the order of 0.15 radius. Taking into account this very large uncertainty, one could postulate that Saturn's dynamo is confined within 0.23 ± 0.15 Rs. This

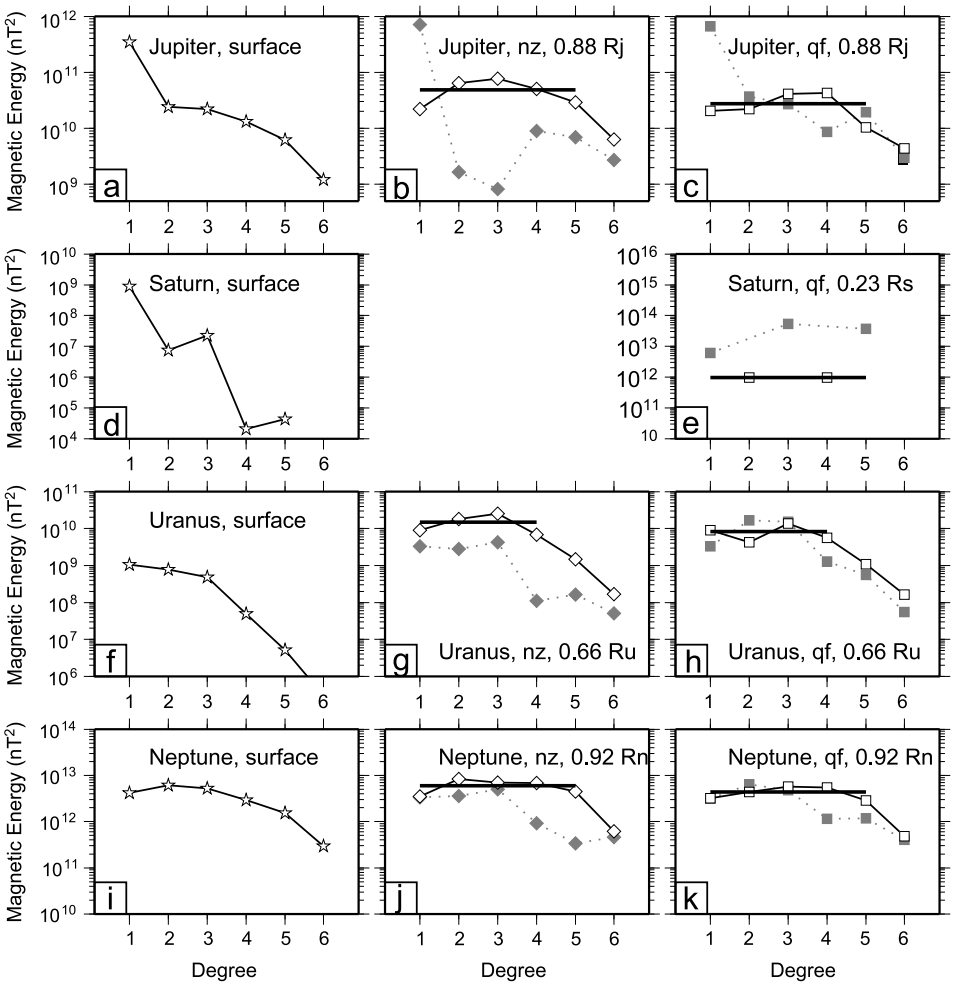

Fig. 5. Magnetic spatial power spectrum for the four giant planets at their surface in the left column, for their non-zonal (open symbols) and zonal (gray closed symbols) in the middle column, and quadrupole (open symbols) and dipole (gray closed symbols) family spectra in the right column at estimated dynamo radii: Jupiter (1, (b), (c)), Saturn ((d), (e)), Uranus ((f), (g), (h)) and Neptune ((i), (j), (k)). Thick horizontal lines represent the non-zonal and quadrupole family expression fit, respectively. For each planet the vertical scale remains identical except for Saturn.

Table 2
Relative radius of the dynamo region on Jupiter (1 Rj = 69 911 km) for increasing N_{max}. Estimates are based on the jovimagnetic field model of Ridley (2012).

N_{max}	3	4	5	6
Power law	0.50	0.61	0.65	0.63
McLeod's rule	0.64	0.74	0.77	0.73
Non-zonal	1.20	1.00	0.88	0.77
Quadrupole family	1.06	1.03	0.89	0.79

Table 3
Relative radius of the dynamo region on Saturn (1 Rs = 60 268 km) for increasing N_{max}. Estimates are based on the magnetic field model of Cao et al. (2012). The non-zonal expression cannot be applied because of the axisymmetric nature of Saturn's magnetic field model.

N_{max}	3	4	5
Power law	0.40	0.21	0.28
McLeod's rule	0.50	0.26	0.33
Non-zonal	N/A	N/A	N/A
Quadrupole family	N/A	0.23	0.23

is much deeper than the molecular-to-metallic transition of hydrogen, but the upper value of this dynamo radius estimate is consistent with an upper non-convective metallic hydrogen layer and in broad agreement with the results of Cao et al. (2012).

5.3. Uranus

Unlike Saturn and Jupiter, interior models of Uranus (and of Neptune, see below) do not predict a molecular-to-metallic transition of hydrogen (Hubbard et al., 1995). Uranus and Neptune are thought to be composed of three layers, namely a solid rocky core surrounded by two homogeneous envelopes of hydrogen, helium and water. The hydrogen atmospheres in Uranus is much smaller than in Jupiter and Saturn, and pressure and temperature conditions necessary for a molecular-to-metallic transition are not met. These inner and outer envelopes only differ by their mass fraction of heavy elements. Nettelmann et al. (2013a) used revised solid-body rotation periods and flattening values to re-investigate the interior of Uranus. They concluded that the radii of the core and of the inner envelope are close to 0.18 and 0.75 Ru, respectively (Uranus radius, 1 Ru = 25 362 km). These recent results are consistent with previous studies (e.g., Podolak et al., 1995; Helled et al., 2011). The dynamo of Uranus probably originates from the inner envelope (Hubbard et al., 1995; Stanley and Bloxham, 2004). At this depth the icy phases become electrically conductive. Only the outer part of this shell would convect (Stanley and Bloxham, 2006).

The magnetic field of Uranus was discovered and measured by Voyager 2 when the spacecraft made a single flyby in 1986 (Connerney et al., 1987). The construction of a global magnetic field model of Uranus is challenging, because of the very limited amount of measurements. We use the field model of

Table 4
Relative radius of the dynamo region on Uranus (1 Ru = 25 362 km) for increasing N_{max}. Estimates are based on the Uranus magnetic field model of Holme and Bloxham (1996).

N_{max}	3	4	5	6
Power law	0.82	0.62	0.51	0.44
McLeod's rule	1.04	0.75	0.61	0.51
Non-zonal	0.86	0.66	0.53	0.43
Quadrupole family	0.74	0.66	0.56	0.47

Table 5
Relative radius of the dynamo region on Neptune (1 Rn = 24 622 km) for increasing N_{max}. Estimates are based on the Neptune magnetic field model of Holme and Bloxham (1996).

N_{max}	3	4	5	6
Power law	1.06	0.94	0.87	0.77
McLeod's rule	1.34	1.15	1.04	0.90
Non-zonal	1.10	1.00	0.93	0.82
Quadrupole family	1.08	1.03	0.94	0.83

Holme and Bloxham (1996), which is similar to that of Connerney et al. (1987), although it is developed to a higher degree ($N_{max} =$ 10 vs. $N_{max} = 3$), and uses the surface heat flow as an additional constraint to regularize the model. Unlike the magnetic field of the Earth and of the giant gas planets, the field of Uranus (and that of Neptune) is not dominated by an axial dipole.

For $N_{max} = 3$, Holme and Bloxham (1996) returned an estimated dynamo region radius of 0.84 Ru using a power law. They restricted their computation to degree 3 as their spectrum falls down above that degree (Fig. 5(f)), due to the smoothing norm they imposed in the inversion. We give in Table 4 the estimated dynamo region radius using the four expressions for N_{max} ranging between 3 and 6. For $N_{max} = 3$ the radius of the dynamo is between 0.74 and 0.86 Ru depending on the expression. Interestingly, the non-zonal and quadrupole family expressions converge for $N_{max} = 4$ (Fig. 5(g) and (h)), with a dynamo radius estimate at 0.66 Ru. Our result is consistent with previous studies, as it would place the top of the dynamo region between 0.66 and 0.86 Ru. This result is within the range of the inner-to-outer envelope transition (Nettelmann et al., 2013a).

5.4. Neptune

The interior structure of Neptune is similar to that of Uranus, with no metallic hydrogen layer. Using the same techniques as for Uranus, Nettelmann et al. (2013a) studied the interior structure of Neptune. Based on their results the radius of the inner envelope (where the dynamo is expected to originate) would be shallower than on Uranus. The rocky core radius is estimated at 0.3 Rn (Neptune radius, 1 Rn = 24 622 km) and that of the inner hydrogen envelope is close to 0.85 Rn (see Nettelmann et al., 2013a, Fig. 4).

The knowledge of Neptune's interior and magnetic field is closely related to that of Uranus. Voyager 2 made also a flyby around Neptune in 1989 (Connerney et al., 1991). The derivation of a global model of its magnetic field is very difficult. The model of Connerney et al. (1991) is computed up to $N_{max} = 8$ but coefficients with n larger than 3 are poorly resolved or unresolved. As for Uranus', modeling the magnetic field of Neptune therefore requires additional constraints for its regularization. In the following we use the model of Holme and Bloxham (1996). This model is derived up to $N_{max} = 16$, but as for Uranus, high degree terms are not reliable. Its spatial power spectrum at Neptune's surface is shown on Fig. 5(i).

For $N_{max} = 3$, Holme and Bloxham (1996) returned a radius of the dynamo region equal to 1.05 Rn using the power law expression. As pointed by the authors, this clearly shows that standard methods fail to correctly estimate the dynamo radius here, because they imply a dynamo radius outside the planet, which is impossible. We give in Table 5 the dynamo radius for varying N_{max}. For $N_{max} = 3$ none of the expressions return a plausible value (radius exceeding 1 Rn). For $N_{max} = 5$ (Fig. 5(j) and (k)) the non-zonal and quadrupole family expressions are very similar and give a dynamo radius close to 0.93 Rn. This estimate decreases to 0.82 Rn for $N_{max} = 6$.

We also use an overdamped model and an underdamped model as presented by Holme and Bloxham (1996), but with different damping parameters. These two alternative models are used to test the sensitivity of our results to the field model error. The effect of damping is to modify the resulting magnetic field model, and thus its spectrum. For $N_{max} = 5$ (6) both non-zonal and quadrupole family expressions return a dynamo radius of 0.96 (resp. 0.86) Rn for the underdamped model, and 0.89 (resp. 0.79) Rn for the overdamped model. The model of Connerney et al. (1991) returns a dynamo radius close to 0.94 when truncated to $N_{max} = 5$. Overall the non-zonal and quadrupole family expressions point towards a dynamo region radius between 0.79 and 0.96 Rn, which is consistent with the shallower inner convecting envelope of Nettelmann et al. (2013a).

6. Concluding remarks

In this study we propose, compare, test and validate two new expressions to fit the magnetic field power spectrum immediately above the region of the dynamo. The first expression relies on the non-zonal part of the spatial geomagnetic power spectrum (i.e., terms with $m \neq 0$), and the second one on the quadrupole family (i.e., $n + m$ even). These expressions are tested using recent models of the geomagnetic field. They offer a satisfying approximation to the form of the spatial geomagnetic power spectrum sub-families. With these high quality models, based on accurate measurements of the Earth's magnetic field, and using these new expressions it is possible to reliably estimate the Earth's dynamo (core) radius using geomagnetic field measurements only. Non-zonal and quadrupole family expressions return dynamo radius between 3486.6 and 3496.7 km, i.e., within less than 15 km of the seismic value. The associated uncertainty, taking into account an estimated error on the Gauss coefficients, is of the order of 5 km. These results can be seen as the most reliable estimates of the Earth's outer core radius using magnetic measurements alone.

A direct application of these expressions is the evaluation of the distance to the magnetic sources on other planets and moons which possess an internal dynamo and where there exists a global model of their internal magnetic field. Other such bodies are Jupiter, Saturn, Uranus and Neptune. For these four giant planets we derive new and independent estimates of their dynamo radii, provided that their dynamo regime is similar to that of the Earth. For Jupiter, Uranus and Neptune we found dynamo radii of 0.88 Rj, 0.66–0.86 Ru, and 0.79–0.96 Rn, respectively. These values are in agreement with the location of inner and outer envelopes within each of these planets as derived from independent studies (e.g., Saumon and Guillot, 2004; Nettelmann et al., 2013a). Overall these new results can be used to further constrain their internal structure. For Saturn, the purely axisymetric nature of the magnetic field restrains us to confidently estimate the dynamo radius.

It should be noted that the quadrupole family expression proposed here relies on a dynamical scenario in which rotational effects dominate and the flow in the dynamo region is organized along axial columns. When convection exceeds a certain threshold the flow becomes more three dimensional and these axial columns break (Kutzner and Christensen, 2002; Christensen and Aubert, 2006; Olson and Christensen, 2006). Columnar flow is likely to prevail in the dynamo regions of Earth, Jupiter and Saturn, which

exhibit axial dipole dominated magnetic fields. However, the non-axial non-dipolar magnetic fields of Uranus and Neptune may suggest that the convection in these planets is strong enough to break axial columns; our quadrupole family expression might not be adequate for these planets. Nevertheless, it is interesting that our results using the two sub-families for each planets converge, including for Uranus and Neptune.

Caution is however required when analyzing the spectra of giant gas planets. Associated magnetic field models do indeed rely on very limited observations, and the different regularization or damping parameters used may affect their spectra, so that specific expressions might be built in the field models (e.g., Connerney, 1993). At this stage we use the existing models; new data from future missions will allow to improve our estimates.

Spherical harmonics models of the magnetic field of Mercury and Ganymede are not yet available, but they will be in the future with the BepiColombo and JUICE missions (Benkhoff et al., 2010; Grasset et al., 2013). Preliminary models based on the MESSENGER mission data show that the internal Hermean magnetic field is dominated by g_1^0 and g_2^0 (Anderson et al., 2012). Our quadrupole family expression could provide a prediction to other coefficients of the field, provided that the radius of the dynamo is known. To maintain a quadrupole family spectrum independent of n above the dynamo, and assuming that non-zonal features of degree 2 are not (yet) supported by the observations, then the power in the axial quadrupole (i.e., g_2^0) would be roughly balanced by the power in the equatorial dipole (i.e., g_1^1 and h_1^1). However, existing models of the Hermean magnetic field are very axial, with a tilt of the dipole lower than 0.8° (Anderson et al., 2012), corresponding to very small g_1^1 and h_1^1. The quadrupole family expression may be non-applicable possibly because rotational effects are less dominant in the case of Mercury. Alternatively, taking into account higher degree terms may change the slope of the observed sub-family spectrum, including its low-end. More elaborated future models will allow testing the existence of such terms in Mercury's core field.

The new expressions we propose can also be used to bring additional constraints on numerical dynamo modeling (Christensen and Wicht, 2008) and to extrapolate the observed magnetic field and its spectrum beyond the limit of crustal magnetic field screening (Finlay and Amit, 2011). Indeed combining both non-zonal and quadrupole family expressions bring constraints on all Gauss coefficients but zonal odd terms. This could also be considered when looking for alternative regularization functions in the inverse problem for computing new planetary magnetic field models (e.g., Holme and Bloxham, 1996).

Finally, other information can be gained by studying the spatial power spectrum of the secular variation (Holme et al., 2011), or the so called secular variation correlation time, which relates the spatial power spectrum of the magnetic field to that of its secular variation (Stacey, 1992; Hulot and Le Mouel, 1994). Several studies proposed scaling laws for the correlation time as a function of the degree n (Christensen and Tilgner, 2004; Lhuillier et al., 2011; Holme et al., 2011; Christensen et al., 2012). As for the R_n series, the dipole term of the correlation time is always underestimated, while the quadrupole term tends to be overestimated (e.g., Harrison, 1994). This could motivate considering a sub-family of this correlation time as proposed in this paper. Assuming our approach is valid, meaning R_n^{nz} and R_n^{qf} are independent of n at the CMB, then the secular variation spectrum, or some of its sub-families should obey to some law.

Acknowledgements

We acknowledge CNES for a financial support through the TOSCA and GTSS committees during the preparation of SWARM and JUICE missions. H.L. was funded by CNES during his stay in LPGNantes. We also thank Victoria Ridley and Richard Holme for sharing their results about the magnetic field models of Jupiter and Neptune, as well as one anonymous reviewer and Richard Holme for constructive reviews. This is IPGP contribution 3536.

Appendix A. Supplementary material

Supplementary material related to this article can be found online at http://dx.doi.org/10.1016/j.epsl.2014.05.013.

References

Amit, H., Olson, P., 2010. A dynamo cascade interpretation of the geomagnetic dipole decrease. Geophys. J. Int. 181, 1411–1427. http://dx.doi.org/10.1111/j.1365-246X.2010.04596.x.

Anderson, B.J., Johnson, C.L., Korth, H., Purucker, M.E., Winslow, R.M., Slavin, J.A., Solomon, S.C., McNutt, R.L., Raines, J.M., Zurbuchen, T.H., 2011. The global magnetic field of Mercury from MESSENGER orbital observations. Science 333. http://dx.doi.org/10.1126/science.1211001.

Anderson, B.J., Johnson, C.L., Korth, H., Winslow, R.M., Borovsky, J.E., Purucker, M.E., Slavin, J.A., Solomon, S.C., Zuber, M.T., McNutt Jr., R.L., 2012. Low-degree structure in Mercury's planetary magnetic field. J. Geophys. Res. 117. http://dx.doi.org/10.1029/2012JE004159.

Aubert, J., Aurnou, J., Wicht, J., 2008. The magnetic structure of convection-driven numerical dynamos. Geophys. J. Int. 172, 945–956.

Backus, G., Parker, R., Constable, C., 1996. Foundations of Geomagnetism. Cambridge University Press, Cambridge, UK.

Baraffe, I., Chabrier, G., Fortney, J., Sotin, C., 2014. Planetary Internal Structures. Arizona Press, Tucson, AZ. 24 pp.

Barraclough, D.R., 1974. Spherical harmonic models of the geomagnetic field for eight epochs between 1600 and 1910. Geophys. J. R. Astron. Soc. 36, 497–513.

Benkhoff, J., van Casteren, J., Hayakawa, H., Fujimoto, M., Laakso, H., Novara, M., Ferri, P., Middleton, H.R., Ziethe, R., 2010. BepiColombo – comprehensive exploration of Mercury: mission overview and science goals. Planet. Space Sci. 58. http://dx.doi.org/10.1016/j.pss.2009.09.020.

Bloxham, J., Jackson, A., 1992. Time-dependent mapping of the magnetic field at the core mantle boundary. J. Geophys. Res. 97, 19537–19563.

Bouligand, C., Hulot, G., Khokhlov, A., Glatzmaier, G.A., 2005. Statistical palaeomagnetic field modelling and dynamo numerical simulation. Geophys. J. Int. 161. http://dx.doi.org/10.1111/j.1365-246X.2005.02613.x.

Buffett, B.A., Christensen, U.R., 2007. Magnetic and viscous coupling at the core–mantle boundary: inferences from observations of the Earth's nutations. Geophys. J. Int. 171. http://dx.doi.org/10.1111/j.1365-246X.2007.03543.x.

Busse, F., 1970. Thermal instabilities in rapidly rotating systems. J. Fluid Mech. 44, 441–460.

Cain, J.C., Wang, Z., Schmitz, D.R., Meyer, J., 1989. The geomagnetic spectrum for 1980 and core-crustal separation. Geophys. J. 97, 443–447.

Cao, H., Russell, C.T., Christensen, U.R., Dougherty, M.K., Burton, M.E., 2011. Saturn's very axisymmetric magnetic field: no detectable secular variation or tilt. Earth Planet. Sci. Lett. 304, 22–28.

Cao, H., Russell, C.T., Wicht, J., Christensen, U.R., Dougherty, M.K., 2012. Saturn's high degree magnetic moments: evidence for a unique planetary dynamo. Icarus 221, 388–394.

Christensen, U.R., Aubert, J., 2006. Scaling properties of convection-driven dynamos in rotating spherical shells and application to planetary magnetic fields. Geophys. J. Int. 166, 97–114.

Christensen, U., Tilgner, A., 2004. Power requirement of the geodynamo from ohmic losses in numerical and laboratory dynamos. Nature 429, 169–171.

Christensen, U.R., Wardinski, I., Lesur, V., 2012. Timescales of geomagnetic secular acceleration in satellite field models and geodynamo models. Geophys. J. Int. 190. http://dx.doi.org/10.1111/j.1365-246X.2012.05508.x.

Christensen, U.R., Wicht, J., 2008. Models of magnetic field generation in partly stable planetary cores: applications to Mercury and Saturn. Icarus 196. http://dx.doi.org/10.1016/j.icarus.2008.02.013.

Civet, F., Tarits, P., 2013. Analysis of magnetic satellite data to infer the mantle electrical conductivity of telluric planets in the solar system. Planet. Space Sci. 84. http://dx.doi.org/10.1016/j.pss.2013.05.004.

Coe, R., Glatzmaier, G., 2006. Symmetry and stability of the geomagnetic field. Geophys. Res. Lett. 33. http://dx.doi.org/10.1029/2006GL027903.

Connerney, J.E.P., 1992. Doing more with Jupiter's magnetic field. In: Rucker, H.O., Bauer, S.J., Kaiser, M.L. (Eds.), Planetary Radio Emissions III, pp. 13–33.

Connerney, J.E.P., 1993. Magnetic fields of the outer planets. J. Geophys. Res. 98. http://dx.doi.org/10.1029/93JE00980.

Connerney, J.E.P., Acuña, M.H., 1982. Jovimagnetic secular variation. Nature 297, 313–315.

Connerney, J.E.P., Acuña, M.H., Ness, N.F., 1987. The magnetic field of Uranus. J. Geophys. Res. 92, 15329–15336.
Connerney, J.E.P., Acuña, M.H., Ness, N.F., 1991. The magnetic field of Neptune. J. Geophys. Res. 96, 19023–19042.
Connerney, J.E.P., Acuña, M.H., Ness, N.F., Satoh, T., 1998. New models of Jupiter's magnetic field constrained by the Io flux tube footprint. J. Geophys. Res. 103, 11929–11940.
Constable, C.G., Parker, R.L., 1988. Statistics of the geomagnetic secular variation for the past 5 m.y. J. Geophys. Res. 93. http://dx.doi.org/10.1029/JB093iB10p11569.
DeRosa, M., Brun, A., Hoeksema, J., 2012. Solar magnetic field reversals and the role of dynamo families. Astrophys. J. 757, 96.
Dougherty, M.K., Balogh, A., Southwood, D.J., Smith, E.J., 1996. Ulysses assessment of the Jovian planetary field. J. Geophys. Res. 101. http://dx.doi.org/10.1029/96JA02385.
Dziewonski, A., Anderson, D., 1981. Preliminary reference Earth model. Phys. Earth Planet. Inter. 25, 297–356.
Finlay, C., Amit, H., 2011. On flow magnitude and field-flow alignment at Earth's core surface. Geophys. J. Int. 186. http://dx.doi.org/10.1111/j.1365-246X.2011.05032.x.
Fortney, J.J., 2007. The structure of Jupiter, Saturn, and exoplanets: key questions for high-pressure experiments. Astrophys. Space Sci. 307, 279–283.
Gauss, C.F., 1839. Allgemaine theorie des erdmagnetismus. Resultate 3, 47 pp.
Grasset, O., Dougherty, M.K., Coustenis, A., Bunce, E.J., Erd, C., Titov, D., Blanc, M., Coates, A., Drossart, P., Fletcher, L.N., Hussmann, H., Jaumann, R., Krupp, N., Lebreton, J.-P., Prieto-Ballesteros, O., Tortora, P., Tosi, F., Van Hoolst, T., 2013. JUpiter ICy moons explorer (JUICE): an ESA mission to orbit Ganymede and to characterise the Jupiter system. Planet. Space Sci. 78. http://dx.doi.org/10.1016/j.pss.2012.12.002.
Grasset, O., Schneider, J., Sotin, C., 2009. A study of the accuracy of mass-radius relationships for silicate-rich and ice-rich planets up to 100 Earth masses. Astrophys. J. 693. http://dx.doi.org/10.1088/0004-637X/693/1/722.
Gubbins, D., Zhang, K., 1993. Symmetry properties of the dynamo equations for palaeomagnetism and geomagnetism. Phys. Earth Planet. Inter. 75, 225–241.
Gudkova, T.V., Zharkov, V.N., 1999. Models of Jupiter and Saturn after Galileo mission. Planet. Space Sci. 47, 1201–1210.
Guillot, T., 1999. A comparison of the interiors of Jupiter and Saturn. Planet. Space Sci. 47, 1183–1200.
Guillot, T., 2005. The interiors of giant planets: models and outstanding questions. Annu. Rev. Earth Planet. Sci. 33, 493–530.
Hagermann, A., 2005. Planetary heat flow measurements. Philos. Trans. R. Soc. Lond. 363. http://dx.doi.org/10.1098/rsta.2005.1664.
Harrison, C., 1994. An alternative picture of the geomagnetic field. J. Geomagn. Geoelectr. 46, 127–142.
Helled, R., Anderson, J.D., Podolak, M., Schubert, G., 2011. Interior models of Uranus and Neptune. Astrophys. J. Lett. 726. http://dx.doi.org/10.1088/0004-637X/726/1/15.
Hide, R., 1978. How to locate the electrically conducting fluid core of a planet from external magnetic observations. Nature 271, 640–664.
Holme, R., Bloxham, J., 1996. The magnetic fields of Uranus and Neptune: methods and models. J. Geophys. Res. 101, 2177–2200.
Holme, R., Olsen, N., Bairstow, F., 2011. Mapping geomagnetic secular variation at the core mantle boundary. Geophys. J. Int. 186. http://dx.doi.org/10.1111/j.1365-246X.2011.05066.x.
Hubbard, W.B., Podolak, M., Stevenson, D.J., 1995. The interior of Neptune. In: Cruikshank, D.P., Matthews, M.S., Schumann, A.M. (Eds.), Neptune and Triton, pp. 109–138.
Hulot, G., Finlay, C.C., Constable, C.G., Olsen, N., Mandea, M., 2010. The magnetic field of planet Earth. Space Sci. Rev. 152. http://dx.doi.org/10.1007/s11214-010-9644-0.
Hulot, G., Le Mouel, J.L., 1994. A statistical approach to the Earth's main magnetic field. Phys. Earth Planet. Inter. 82, 167–183.
Jault, D., 2008. Axial invariance of rapidly varying diffusionless motions in the Earth's core interior. Phys. Earth Planet. Inter. 166. http://dx.doi.org/10.1016/j.pepi.2007.11.001.
Johnson, C.L., Purucker, M.E., Korth, H., Anderson, B.J., Winslow, R.M., Al Asad, M.M.H., Slavin, J.A., Alexeev, I.I., Phillips, R.J., Zuber, M.T., Solomon, S.C., 2012. MESSENGER observations of Mercury's magnetic field structure. J. Geophys. Res. 117. http://dx.doi.org/10.1029/2012JE004217.
Kennett, B.L.N., Engdahl, E.R., Buland, R., 1995. Constraints on seismic velocities in the Earth from travel-times. Geophys. J. Int. 122, 108–124.
Kono, M., Tanaka, H., Tsunakawa, H., 2000. Spherical harmonic analysis of paleomagnetic data: the case of linear mapping. J. Geophys. Res. 105. http://dx.doi.org/10.1029/1999JB900050.
Kutzner, C., Christensen, U.R., 2002. From stable dipolar towards reversing numerical dynamos. Phys. Earth Planet. Inter. 131. http://dx.doi.org/10.1016/S0031-9201(02)00016-X.
Langel, R.A., 1987. The main field. In: Jacobs, J.A. (Ed.), Geomagnetism, vol. 1. Academic Press, pp. 249–512. Ch. 4.
Langel, R.A., Estes, R.H., 1982. A geomagnetic field spectrum. Geophys. Res. Lett. 9, 250–253.
Lhuillier, F., Fournier, A., Hulot, G., Aubert, J., 2011. The geomagnetic secular variation timescale in observations and numerical dynamo models. Geophys. Res. Lett. 38. http://dx.doi.org/10.1029/2011GL047356.
Lowes, F.J., 1966. Mean square values on the sphere of spherical harmonic vector fields. J. Geophys. Res. 71, 2179.
Lowes, F.J., 1974. Spatial power spectrum of the main geomagnetic field and extrapolation to the core. Geophys. J. R. Astron. Soc. 36, 717–730.
Lowes, F., 2007. Geomagnetic spectrum, spatial. In: Gubbins, D., Herrero-Bervera, E. (Eds.), Enc. Geomag. Paleomag. Springer, The Netherlands, pp. 350–353.
McLeod, M.G., 1996. Spatial and temporal power spectra of the geomagnetic field. J. Geophys. Res. 101, 2745–2763.
Mocquet, A., Rosenblatt, P., Dehant, V., Verhoeven, O., 2011. The deep interior of Venus, Mars, and the Earth: a brief review and the need for planetary surface-based measurements. Planet. Space Sci. 59. http://dx.doi.org/10.1016/j.pss.2010.02.002.
Ness, N.F., Acuña, M.H., Behannon, K.W., Burlaga, L.F., Connerney, J.E.P., Lepping, R.P., Neubauer, F.M., 1982. Magnetic field studies by Voyager 2 – preliminary results at Saturn. Science 215, 558–563.
Ness, N.F., Acuña, M.H., Lepping, R.P., Connerney, J.E.P., Behannon, K.W., Burlaga, L.F., Neubauer, F.M., 1981. Magnetic field studies by Voyager 1 – preliminary results at Saturn. Science 212, 211–217.
Nettelmann, N., Helled, R., Fortney, J.J., Redmer, R., 2013a. New indication for a dichotomy in the interior structure of Uranus and Neptune from the application of modified shape and rotation data. Planet. Space Sci. 77. http://dx.doi.org/10.1016/j.pss.2012.06.019.
Nettelmann, N., Püstow, R., Redmer, R., 2013b. Saturn layered structure and homogeneous evolution models with different EOSs. Icarus. http://dx.doi.org/10.1016/j.icarus.2013.04.018.
Olson, P., 2007. Core dynamics – overview. In: Kono, M. (Ed.), Treatise on Geophysics, vol. 8. Elsevier, Amsterdam, The Netherlands.
Olson, P., Christensen, U.R., 2006. Dipole moment scaling for convection-driven planetary dynamos. Earth Planet. Sci. Lett. 250. http://dx.doi.org/10.1016/j.epsl.2006.08.008.
Olson, P., Christensen, U., Glatzmaier, G., 1999. Numerical modeling of the geodynamo: mechanisms of field generation and equilibration. J. Geophys. Res. 104. http://dx.doi.org/10.1029/1999JB900013.
Pinheiro, K., Jackson, A., 2008. Can a 1-D mantle electrical conductivity model generate magnetic jerk differential time delays? Geophys. J. Int. 173. http://dx.doi.org/10.1111/j.1365-246X.2008.03762.x.
Podolak, M., Weizman, A., Marley, M., 1995. Comparative models of Uranus and Neptune. Planet. Space Sci. 43, 1517–1522.
Ridley, V.A., 2012. Jovimagnetic secular variation. Ph.D. thesis. The University of Liverpool, UK.
Ridley, V.A., Holme, R., 2012. The Magnetic Field and Secular Variation of Jupiter. EGU General Assembly Conference Abstracts, vol. 14.
Roberts, P.H., 1971. Dynamo theory. In: Reid, W.H. (Ed.), Mathematical Problems in the Geophysical Sciences, Am. Math. Soc.
Roberts, P., Jones, C., Calderwood, A., 2003. Energy Fluxes and Ohmic Dissipation in the Earth's Core. CRC Press, London, UK, pp. 100–129.
Saumon, D., Guillot, T., 2004. Shock compression of deuterium and the interiors of Jupiter and Saturn. Astrophys. J. Lett. 609, 1170–1180.
Smith, E.J., Davis Jr., L., Jones, D.E., Coleman Jr., P.J., Colburn, D.S., Dyal, P., Sonett, C.P., 1975. Jupiter's magnetic field, magnetosphere, and interaction with the solar wind – Pioneer 11. Science 188, 451–455.
Smith, E.J., Davis, L., Jones, D.E., Coleman, P.J., Colburn, D.S., Dyal, P., Sonett, C.P., 1980. Saturn's magnetic field and magnetosphere. Science 207, 407–410.
Stacey, F.D., 1992. Physics of the Earth. Brookfield Press, Brisbane, Australia.
Stanley, S., Bloxham, J., 2004. Convective-region geometry as the cause of Uranus' and Neptune's unusual magnetic fields. Nature 428. http://dx.doi.org/10.1038/nature02376.
Stanley, S., Bloxham, J., 2006. Numerical dynamo models of Uranus' and Neptune's magnetic fields. Icarus 184. http://dx.doi.org/10.1016/j.icarus.2006.05.005.
Stanley, S., Mohammadi, A., 2008. Effects of an outer thin stably stratified layer on planetary dynamos. Phys. Earth Planet. Inter. 168. http://dx.doi.org/10.1016/j.pepi.2008.06.016.
Stevenson, D.J., 1980. Saturn's luminosity and magnetism. Science 208, 746–748.
Stevenson, D.J., 1983. Planetary magnetic fields. Rep. Prog. Phys. 46, 555–620.
Taylor, G., 1971. Thermal instabilities in rapidly rotating systems. Proc. R. Soc. Lond. 93, 92–113.
Verhoeven, O., Mocquet, A., Vacher, P., Rivoldini, A., Menvielle, M., Arrial, P.A., Choblet, G., Tarits, P., Dehant, V., Van Hoolst, T., 2009. Constraints on thermal state and composition of the Earth's lower mantle from electromagnetic impedances and seismic data. J. Geophys. Res. 114. http://dx.doi.org/10.1029/2008JB005678.
Voorhies, C.V., 2004. Narrow-scale flow and a weak field by the top of Earth's core: evidence from Ørsted, Magsat, and secular variation. J. Geophys. Res. 109. http://dx.doi.org/10.1029/2003JB002833.
Voorhies, C.V., Sabaka, T.J., Purucker, M.E., 2002. On magnetic spectra of Earth and Mars. J. Geophys. Res. 107. http://dx.doi.org/10.1029/2001JE001534.
Xu, W.-Y., 2000. Unusual behaviour of the IGRF during the 1945–1955 period. Earth Planets Space 52, 1227–1233.

Yu, Z.J., Leinweber, H.K., Russell, C.T., 2010. Galileo constraints on the secular variation of the Jovian magnetic field. J. Geophys. Res. 115. http://dx.doi.org/10.1029/2009JE003492.

Zmuda, A., 1971. The international geomagnetic reference field 1965.0, introduction. Bull. Int. Assoc. Geomagn. Aeron. 28, 148–152.

Zuber, M.T., Montési, L.G.J., Farmer, G.T., Hauck, S.A., Andreas Ritzer, J., Phillips, R.J., Solomon, S.C., Smith, D.E., Talpe, M.J., Head, J.W., Neumann, G.A., Watters, T.R., Johnson, C.L., 2010. Accommodation of lithospheric shortening on Mercury from altimetric profiles of ridges and lobate scarps measured during MESSENGER flybys 1 and 2. Icarus 209. http://dx.doi.org/10.1016/j.icarus.2010.02.026.